Electronic Supplementary Information (ESI)

Excavated cubic platinum-iridium alloy nanocrystals with high-index facets as highly efficient electrocatalyst in N_2 fixation to NH_3

Yu-Jie Mao,[a,b] Lu Wei,*[,a] Xin-Sheng Zhao,[a] Yong-Sheng Wei,[a] Jian-Wei Li,[a] Tian Sheng,*[,c] Fu-Chun Zhu,[b] Na Tian,[b] Zhi-You Zhou,[b] Shi-Gang Sun*[,b]

[a] School of Physics and Electronic Engineering, Jiangsu Normal University, Xuzhou 221116, China

[b] State Key Lab of PCOSS, College of Chemistry and Chemical Engineering, Xiamen University, Xiamen 361005, China

[c] College of Chemistry and Materials Science, Anhui Normal University, Wuhu, 241000, China

* Corresponding authors:

E-mail: lwei057@jsnu.edu.cn; sgsun@xmu.edu.cn; tsheng@ahnu.edu.cn

Fax: +86-592-2180181

Tel: +86-516 83500485; +86-592-2180181

1. Experimental section

Chemical. Potassium chloroplatinate (K_2PtCl_6, AR reagent), Iridium(III)chloride hydrateurea ($IrCl_3 \cdot xH_2O$, GR reagent, 99.9%), urea ($CO(NH_2)_2$, AR reagent, >99%), choline chloride ($HOC_2H_4N(CH_3)_3Cl$, 99%), hydrochloric acid (HCl, AR reagent, 36.0~38.0%) and perchloric acid ($HClO_4$, GR reagent), sodium hydroxide (NaOH), salicylic acid, sodium citrate, sodium hypochlorite aqueous solution (NaClO), sodium nitroferricyanide ($C_5FeN_6Na_2O$), para-(dimethylamino) benzaldehyde were purchased from Sinopharm Chemical Reagent Co. Ltd (Shanghai, China). 20 wt% Pt/C catalyst was purchased from Alfa Aesar.

Preparation of deep eutectic solvent. The typical preparation of DES was described in detail in previous reports.[S1-S3] In short, purified ChCl and urea were mixed in a beaker at a defined ratio (ChCl: urea = 1: 2, molar ratio) and stirred at 80 ℃ until a uniform colorless liquid formed. The as-prepared DES was then stored in a vacuum of 80 ℃ before use.

Synthesis of excavated cubic Pt-Ir alloy NCs. The excavated cubic Pt-Ir alloy NCs were achieved by electrodeposition in a standard three-electrode cell connected to a CHI 760E electrochemical workstation (Shanghai Chenhua Instrumental Co., Ltd., China), with a platinum wire counter electrode and a platinum quasi-reference electrode. The working electrode was a glassy carbon disk (GC, Φ = 6 mm). Prior to each electrodeposition, the GC was polished using a fine mechanical Al_2O_3 with powder size of 1.0 and 0.3 μm and then cleaned ultrasonically in an ultrapure water bath. In detail, the excavated cubic $Pt_{93}Ir_7$ alloy NCs were electrodeposited form a 9.26 mM K_2PtCl_6 + 0.74 mM $IrCl_3$ of ChCl-urea based DES solution. The Pt-Ir alloy NCs with different compositions ($Pt_{96}Ir_4$, $Pt_{90}Ir_{10}$ and $Pt_{88}Ir_{12}$) and pure Pt NCs were electrodeposited form the 9.62 mM K_2PtCl_6 + 0.38 mM $IrCl_3$, 8.93 mM K_2PtCl_6 + 1.07 mM $IrCl_3$, 8.62 mM K_2PtCl_6 + 1.38 mM $IrCl_3$ and 10 mM K_2PtCl_6 of ChCl-urea based DES solutions, respectively. All samples were electrodeposited by cyclic voltammetry with

a potential scan from –0.20 to –1.50 V (vs. Pt quasi-reference electrode) at 50 mV s^{-1} at 80 ℃ for 60 cycles.

Alloy structure and composition characterizations. Scanning electron microscopy (SEM) images of concave cubic PtIr alloy NCs were analyzed using SU8010 electron microscope. Transmission electron microscopy (TEM) and high-resolution TEM (HR-TEM) measurements were carried out on a FEI Tecnai-F30 electron microscope with an operating voltage of 300 kV. The energy-dispersive X-ray spectroscopy (EDS) and elemental mapping tests were performed on the FEI Tecnai-F30 TEM.

Electrocatalytic nitrogen reduction measurements. The NRR activity tests were conducted in a standard three-electrode cell containing 30 mL of 1 mM HCl solution under ambient conditions, in which the cathode and anode was separated by the Nafion-211 membrane. Before NRR test, the Nafion 211 membrane was heated in 5 % H_2O_2, 0.5 M H_2SO_4, and ultrapure water at 80 ℃ for 1 h, respectively. A platinum slice and a saturated calomel electrode (SCE) were used as the counter and reference electrodes, respectively. For electrochemical N_2 reduction, chronoamperometry tests were carried out at different potentials in N_2-saturated 1 mM HCl solution, which was purged with N_2 during the electrolysis. To ensure the tests with N_2-saturated conditions, the solution was purged with N_2 for 1 hr before each measurement. The NRR products were spectrophotometrically determined by the indophenol indicator and the Watt and Chrisp methods.[S4,S5] The calibration curve for the NH_3 meter is shown in Figure S6. The NH_3 yield rate (*r*) and Faradaic efficiency (FE) are calculated by the following equations:

$$r(NH_3) = \frac{[NH_3] \times V}{t \times A} \quad (1)$$

$$FE(NH_3) = \frac{Q_{NH_3}}{Q_{total}} \frac{3 \times 96500 \times [NH_3] \times V}{\int idt} \quad (2)$$

Where *A* is the electrochemically active surface area, which was calculated from the electric charge of hydrogen adsorption/desorption on Pt-Ir alloy surface.

Computational methods. All electronic structure calculations were performed using the SIESTA package with Troullier-Martins norm conserving pseudopotentials.[S6-S8] The exchange-correlation functional utilized was at the generalized gradient approximation (GGA) level with Perdew-Burke-Ernzerhof (PBE).[S9] A double-ξ plus polarization (DZP) basis set was employed and the orbital-confirming cutoff was determined from an energy shift of 0.01 eV. The van der waals interactions were considered by vdw-DF functional by Dion et al.[S10,S11] A four-layer Pt(210), Pt(310) and Pt(410) slab was modeled by a *p*(2×1) supercell with 16, 24 and 32 Pt atoms. For modelling the Ir modified Pt surfaces, one Pt atom at the step site was replaced by one Ir atom. The models are shown in Figure S10. The bottom two layers were fixed at their bulk positions and other atoms were allowed to move during optimizations. The cut-off energy for the real space grid was 450 eV. A 4×4×1 Monkhorst-Pack *k*-point mesh was used. The vacuum region was ~15 Å to eliminate interactions between slabs in the z direction.

The free energy of species was obtained from G = E + ZPE - TS, where E is the total energy of species, S is the entropy and ZPE is the zero point energy at room temperature (300 K). The reaction free energy of AH → A + H^+ + e^- was calculated as ΔG = G(A) + G(H^+ + e^-) – G(AH). At the electrode potential of 0 V, pH = 0 ([H^+] = 1M), at 298 K, due to the equilibrium of H^+ + e^- → ½ H_2, we can use the free energy of ½ H_2 in the gas phase to replace that of H^+ + e^-.[S12] All vibrational frequencies of adsorbates, ν_i(Hz), were calculated based on the harmonic oscillators approximation.[S13] The adsorption energy was defined as: E_{ad} = E(ad/surf) - E(ad) - E(surf), where E(ad/surf), E(ad), and E(surf) are the total energies of the adsorbate binding to surface, free adsorbate in vacuum and clean surface, respectively. For reactions involving adsorption and desorption, water effects were considered approximately by one water molecule at the same site.

2. The electrodeposition behaviors of Pt and Ir in DES

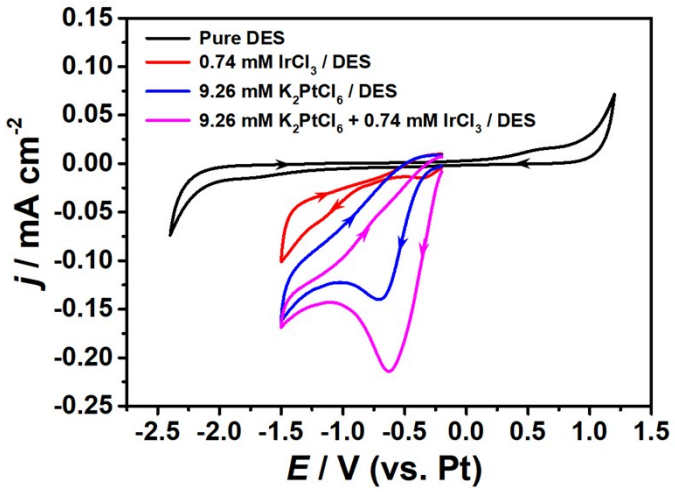

Fig. S1. Cyclic voltammograms of GC substrate in different solutions at 80 ºC. Scan rate: 50 mV s^{-1}.

For insight into the electrodeposition behaviors of Pt and Ir, the cyclic voltammograms (CVs) of a GC electrode in the pure ChCl-urea based DES (black curve) and ChCl-urea based DES solutions containing 0.74 mM $IrCl_3$ (red curve), 9.26 mM K_2PtCl_6 (blue curve) and 9.26 mM K_2PtCl_6 + 0.74 mM $IrCl_3$ (pink curve) were performed at a scan rate of 50 mV s^{-1} at 80 ºC, as illustrated in Fig. S1. From the black curve it can be clearly observed that the ChCl-urea based DES exhibits an electrochemical stability window of around 3 V on GC, ranging from –2 V to 1 V with respect to the Pt quasi-reference electrode. The red curve shows that there are two cathodic peaks at –0.35 V and –1.15 V, corresponding Ir deposition on GC. From the blue curve a distinct reduction processes is observed at –0.70 V, which is attributed to Pt deposition. The pink curve was recorded in a 9.26 mM K_2PtCl_6 + 0.74 mM $IrCl_3$ of ChCl-urea based DES solution. It is worth noting that, except for the higher cathodic peak current and more positive cathodic peak potential (–0.62 V), the feature of CV profile is similar to that obtained in a 9.26 mM K_2PtCl_6 of ChCl-urea based DES solution (blue curve). Above observes indicate that, within the electrochemical stability range of ChCl-urea based DES, Pt and Ir can be coelectrodeposited and effectively form alloy on the GC electrode without the interference of any electrolyte decomposition reaction.

3. SEM and EDX characterizations

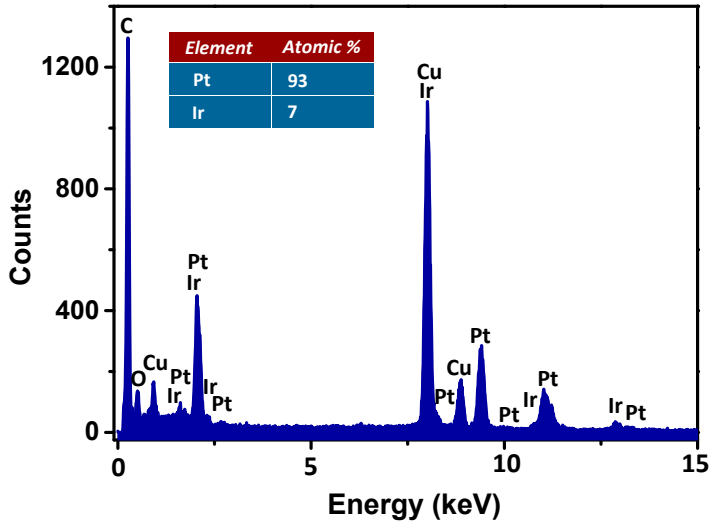

Fig. S2. EDX spectrum of concave cubic $Pt_{93}Ir_7$ alloy NCs.

Table S1. The calculated values for the angles of different high-index planes of Miller indices {*hk*0} with the {100} plane.

{*hk*0}	{910}	{810}	{710}	{610}	{510}
ϑ / º	6.34	7.12	8.13	9.46	11.31

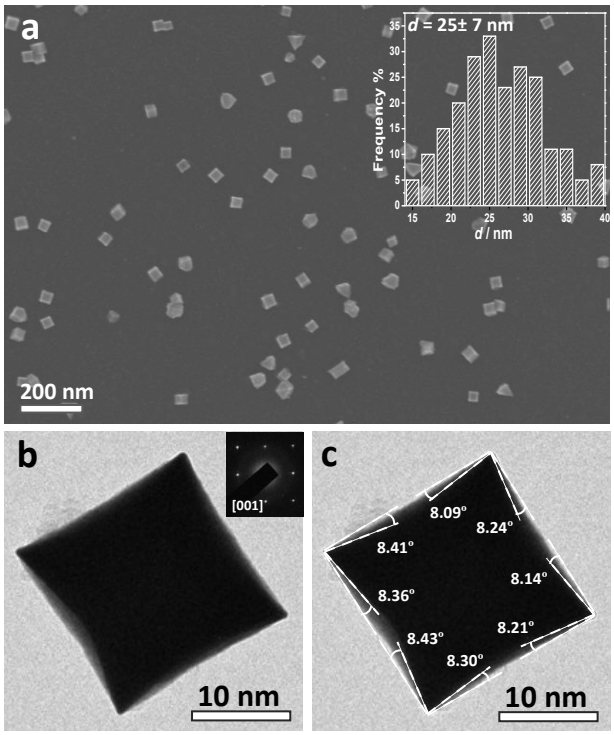

Fig. S3. (a) SEM image, (b) TEM image and (c) measured angles of a single excavated cubic Pt NC oriented along the [001] direction. The inset is SAED pattern..

Fig. S3(a) shows a typical SEM image of excavated cubic Pt NCs and their size is measured to be 27 ± 7 nm (see the inset of Figure S3(a)). Fig. S3(b) displays a high-resolution TEM image of a single excavated cubic Pt NC projected along the [001] direction that was confirmed by the corresponding selected-area electron diffraction (SAED) pattern (see the inset of Fig. S3(b)). The angles between the facets of the projected excavated nanocube and the {100} facets of an ideal cube were measured to be 8.41°, 8.09°, 8.24°, 8.14°, 8.21°, 8. 30°, 8.43°, 8.36° (Fig. S3(c)). Comparing the measured angles with the ideal values (Table S1), it is indicated that the as-prepared excavated cubic Pt NCs are mainly enclosed by high-index {710} facets.

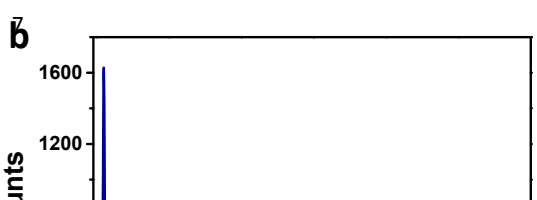

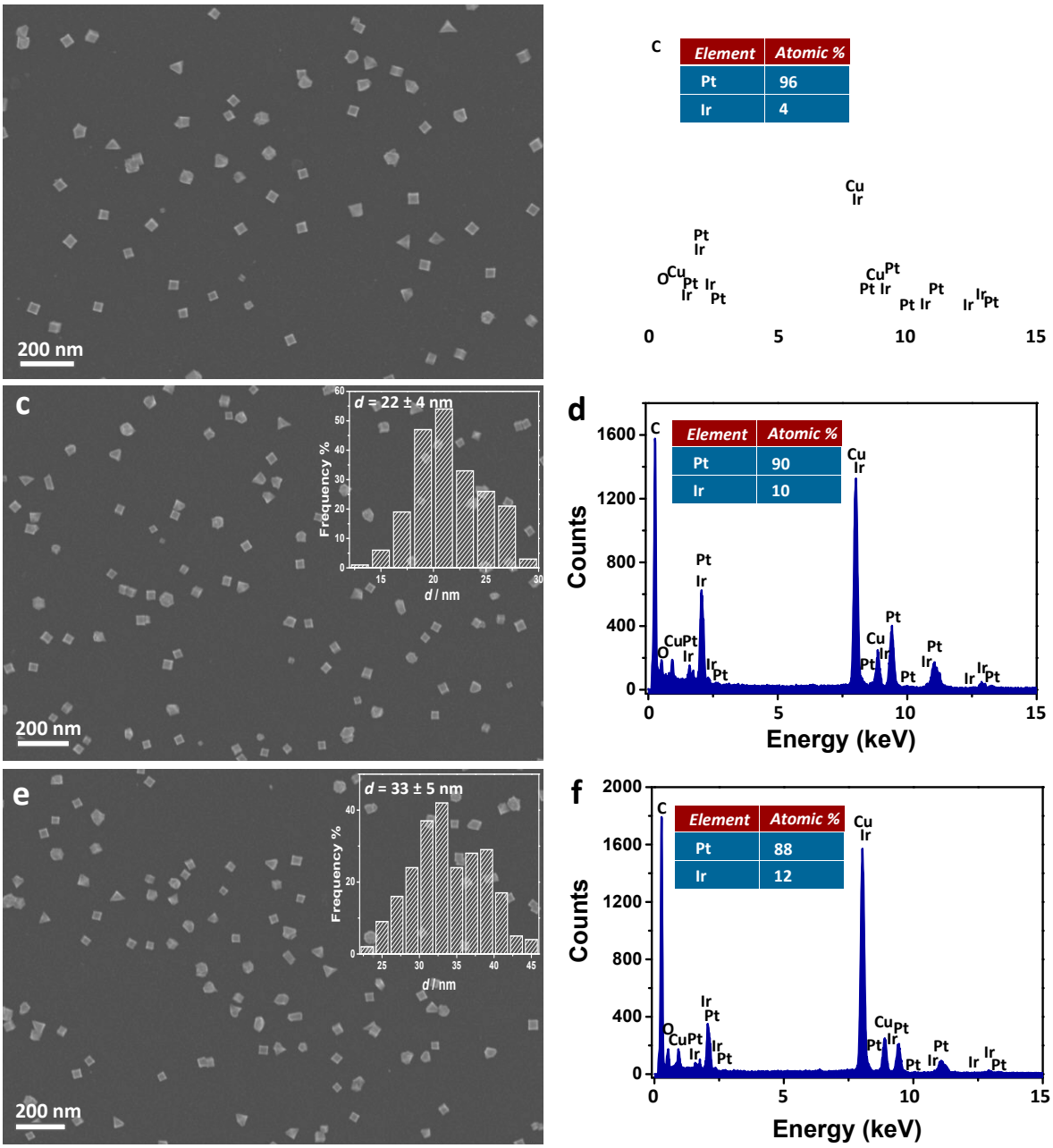

Fig. S4. SEM images (a, c, e) and corresponding energy-dispersive X-ray spectroscopy (b, d, f) of the excavated cubic pure Pt and Pt-Ir alloy NCs electrodeposition from different concentration of K_2PtCl_6 and $IrCl_3$ DES solutions: (a and b) 10 mM K_2PtCl_6, (c and d) 9.62 mM K_2PtCl_6 + 0.38 mM $IrCl_3$, (e and f) 8.93 mM K_2PtCl_6 + 1.07 mM $IrCl_3$, (d) 8.62 mM K_2PtCl_6 + 1.38 mM $IrCl_3$.

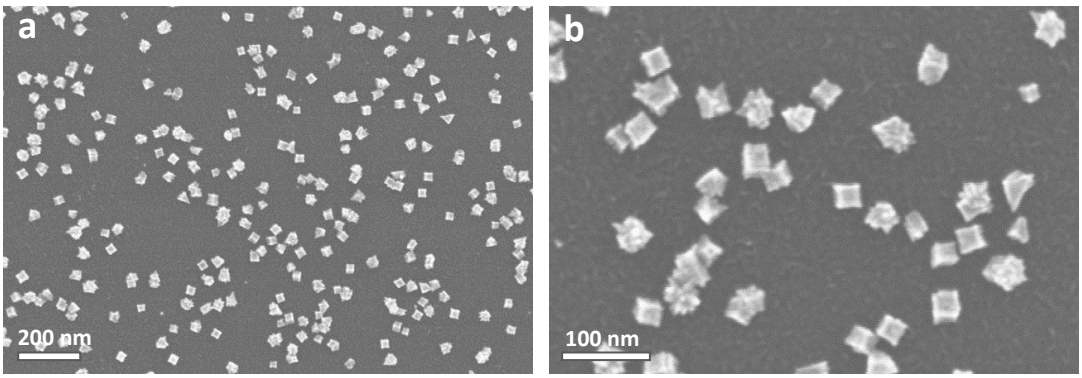

Fig. S5. SEM images of Pt-Ir alloy electrodeposition from a DES solution containing 8.33 mM K_2PtCl_6 + 1.67 mM $IrCl_3$.

4. UV-Vis absorption spectra and electrocatalytic characterizations

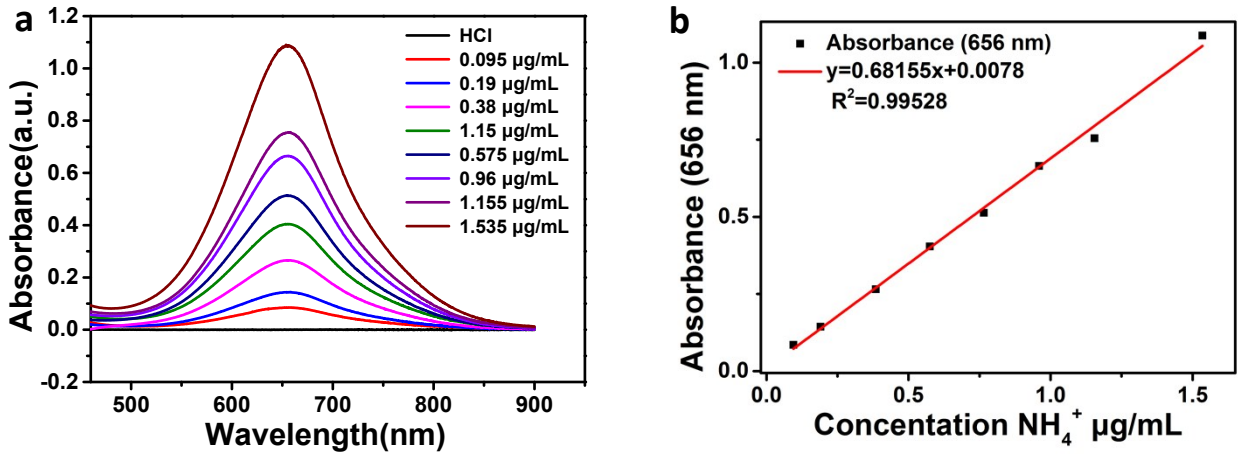

Fig. S6. Absolute calibration of the indophenol blue method using ammonium chloride solutions of known concentration as standards. (a) UV-Vis curves of indophenol assays with NH_4^+ ions after incubated for 1 hour at room temperature; (b) calibration curve used for estimation of NH_3 by NH_4^+ ion concentration. The absorbance at 656 nm was measured by UV-Vis spectrophotometer, and the fitting curve shows good linear relation of absorbance with NH_4^+ ion concentration (y = 0.6815x + 0.0078, R^2 = 0.99528) of three times independent calibration curves.

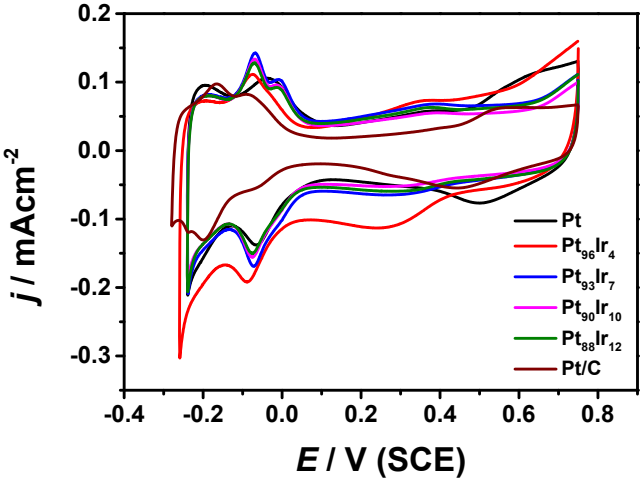

Fig. S7. CV profiles of excavated cubic Pt, $Pt_{96}Ir_4$, $Pt_{93}Ir_7$, $Pt_{90}Ir_{10}$, $Pt_{88}Ir_{12}$ NCs and commercial Pt/C catalysts in 0.1 M $HClO_4$ solution. Scan rate: 50 mV s^{-1}.

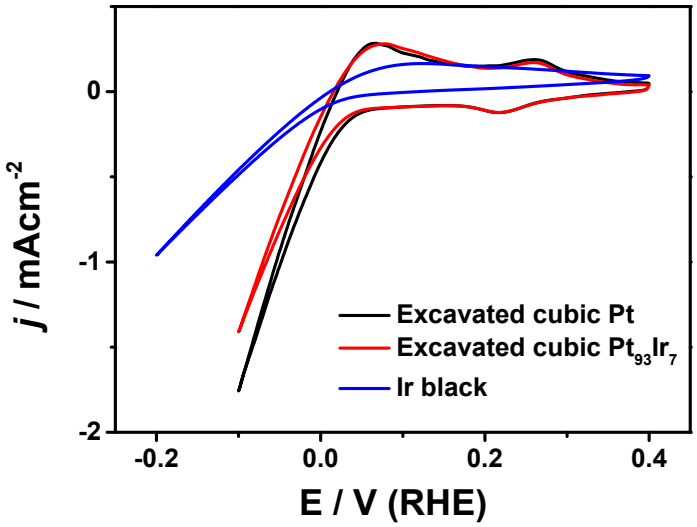

Fig. S8. HER tests of excavated cubic $Pt_{93}Ir_7$, Pt NCs and Ir black in 1 mM HCl solution. Scan rate: 50 mV s^{-1}.

Fig. S8 displays electrochemical activity of HER on excavated cubic $Pt_{93}Ir_7$, Pt NCs and Ir black in 1 mM HCl solution. It can be seen that the electrochemical activity of HER on Ir black (blue curve) is rather worse than that on excavated cubic Pt NCs (black curve). When Ir was introduced into the Pt stepped surface, it is found that the excavated cubic $Pt_{93}Ir_7$ NCs can effectively suppress the HER (red curve). This result indicates that the presence of Ir on such Pt stepped surface is able to suppress the HER.

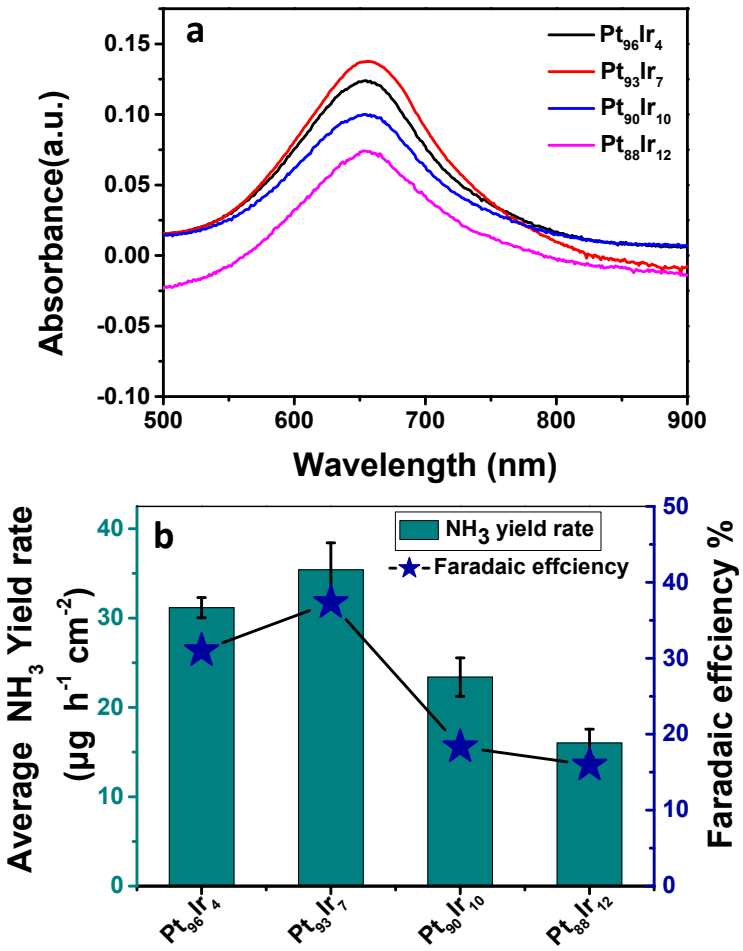

Fig. S9. (a) UV-Vis absorption spectra and (b) Yield rate of NH_3 (Dark Cyan) and Faradaic efficiency (Royal blue) on a series of excavated cubic Pt-Ir alloy NCs.

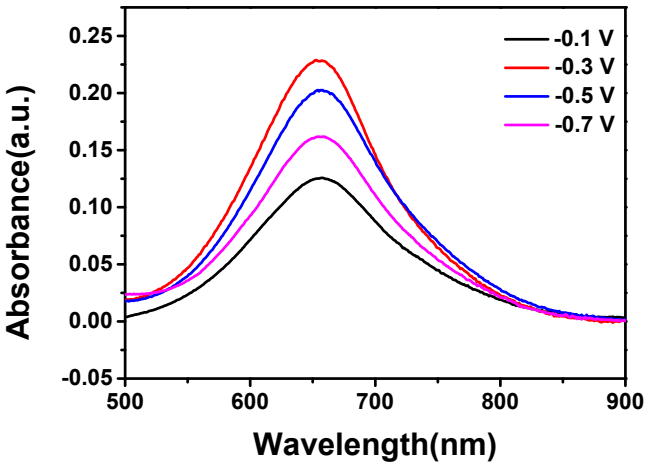

Fig. S10. UV-Vis absorption spectra of the electrolytes stained with indophenol blue indicator after NRR electrolysis on $Pt_{93}Ir_7$ in 1 mM HCl solution at different potentials.

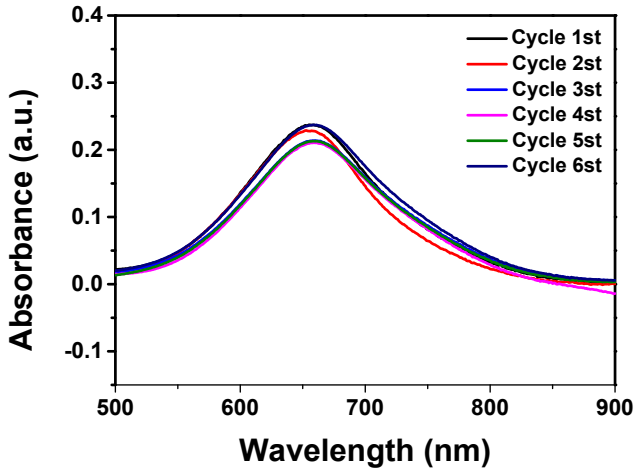

Fig. S11. UV-Vis absorption spectra of the electrolytes stained with indophenol blue indicator after NRR electrolysis on $Pt_{93}Ir_7$ in 1 mM HCl solution for different cycling tests.

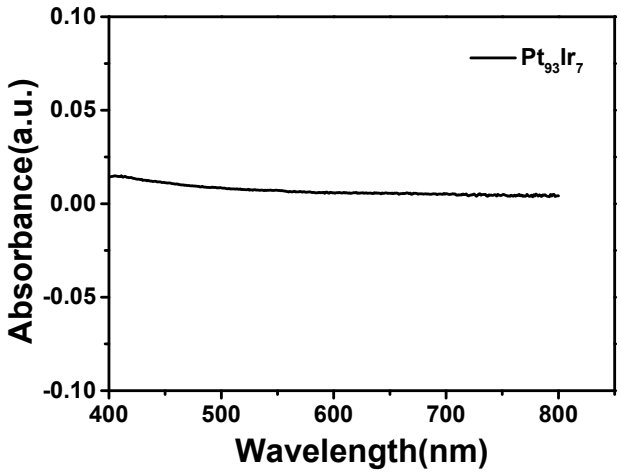

Fig. S12. UV-Vis absorption spectra of $Pt_{93}Ir_7$ alloy NCs with the Watt and Chrisp method.

Table S2. Comparison of the electrocatalytic property for NRR on excavated cubic $Pt_{93}Ir_7$ with reported catalysts

under ambient conditions.

Electrocatalysts	Electrolytes	r_{NH3}	FE (%)	Ref.
Excavated cubic $Pt_{93}Ir_7$	**1mM HCl**	**28 μg h^{-1} cm^{-2}**	**40.8**	**This Work**
Mo nanofilm	0.01 M H_2SO_4	1.89 μg h^{-1} cm^{-2}	0.72	S14
Fe_2O_3-CNT	KHO_3	0.22 μg h^{-1} cm^{-2}	0.15	S15
Au nanorods	0.1 M KOH	1.6 μg h^{-1} cm^{-2}	3.88	S16
AuHNCs	0.5 M $LiSO_4$	3.9 μg h^{-1} cm^{-2}	30.2	S17
Fe_3O_4/Ti	0.1 M Na_2SO_4	5.6 × 10^{-11} mol s^{-1} cm^{-2}	2.6	S18
Pd/C	0.1M PBS	4.5 μg h^{-1} cm^{-2}	8.2	S19
N-doped carbonnanospikes	0.25 M$LiClO_4$	97.18 μg h^{-1} cm^{-2}	11.56	S20
ZIF-derivedcarbon	0.1 M KOH	57.8 μg h^{-1} cm^{-2}	10.20	S21
MoN	0.1 M HCl	3.01×10^{-10} mol s^{-1} cm^{-2}	1.15	S22
MoS_2 /CC	0.1 M Na_2SO_4	4.94 μg h^{-1} cm^{-2}	1.17	S23
VN/TM	0.1 M HCl	8.40×10^{-11} mol s^{-1} cm^{-2}	2.25	S24
PEBCD/C	0.5 M Li_2SO_4	1.58 μg h^{-1} cm^{-2}	2.85	S25
Ag nanosheet	0.1 M HCl	4.62×10^{-11} mol s^{-1} cm^{-2}	4.8	S26
SnO_2/CC	0.1 M Na_2SO_4	4.03μg h^{-1} cm^{-2}	2.17	S27
Boron-Doped Graphene	0.05 M H_2SO_4	9.8 μg h^{-1} cm^{-2}	10.8	S28
Fe/Fe_3O_4	0.1 M PBS	8.08×10^{-11} mol s^{-1} cm^{-2}	8.29	S29
MoO_3	0.1 M HCl	29.43μg h^{-1} $mg^{-1}_{cat.}$	1.9	S30
Mo_2N	0.1 M HCl	78.4 μg h^{-1} $mg^{-1}_{cat.}$	4.5	S31
β- FeOOH	0.5 M $LiClO_4$	23.32 μg h^{-1} $mg^{-1}_{cat.}$	6.7	S32
TiO_2-rGO	0.1 M Na_2SO_4	5.13 μg h^{-1} $mg^{-1}_{cat.}$	3.3	S33
γ-Fe_2O_3nanoparticles	0.1 M KOH	0.212 μg h^{-1} $mg^{-1}_{cat.}$	1.9	S34
N-doped porouscarbon	0.05 M H_2SO_4	23.8 μg h^{-1} $mg^{-1}_{cat.}$	1.42	S35
$Bi_4V_2O_{11}$ /CeO_2	0.1 M HCl	23.21 μg h^{-1} $mg^{-1}_{cat.}$	10.16	S36
hollow Cr_2O_3microspheres	0.1 M Na_2SO_4	25.3 μg h^{-1} $mg^{-1}_{cat.}$	6.78	S37
B_4C	0.1 M HCl	26.57 μg h^{-1} $mg^{-1}_{cat.}$	15.95	S38
Nb_2O_5nanofiber	0.1 M HCl	43.6 μg h^{-1} $mg^{-1}_{cat.}$	9.26	S39
Black Phosphorus	0.01 M HCl	31.37 μg h^{-1} $mg^{-1}_{cat.}$	5.07	S40
Atomically dispersed Mo	0.1 M NaOH	34.6 μg h^{-1} $mg^{-1}_{cat.}$	14.6	S41
Fe-N/C-CNT	0.1 M KOH	34.86 μg h^{-1} $mg^{-1}_{cat.}$	9.28	S42
$Pd_{0.2}Cu_{0.8}$/rGO	0.1 M KOH	2.8 μg h^{-1} $mg^{-1}_{cat.}$	4.5	S43
Ru Single-Atom	HCl	3.665 mg h^{-1} $mg^{-1}_{cat.}$	21	S44
N-doped porous C	0.1 M KOH	15.7μg h^{-1} $mg^{-1}_{cat.}$	1.45	S45
Au flowers	0.1 M HCl	25.57μg h^{-1} $mg^{-1}_{cat.}$	6.05	S46
Au-TiO_2	0.1 M HCl	21.4 μg h^{-1} $mg^{-1}_{cat.}$	8.11	S47
Au/CeO_X-RGO	0.1 M HCl	8.3 μg h^{-1} $mg^{-1}_{cat.}$	10.1	S48
Rh nanosheet	0.1 M KOH	23.88 μg h^{-1} $mg^{-1}_{cat.}$	0.7	S49

5. Density functional theory (DFT) calculations

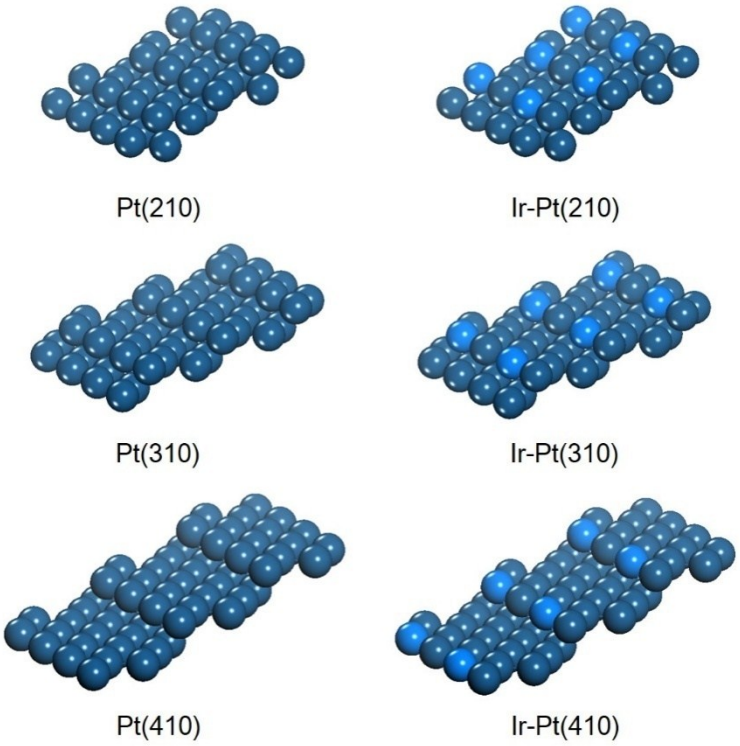

Fig. S13. Models of Pt and Ir modified Pt step surfaces

Table S3. Calculated reaction energies (unit in eV) of elementary steps for nitrogen reduction reactions on Pt(210), Pt(310), Pt(410) and Ir modified Pt(210), Pt(310), Pt(410), respectively.

	Pt(210)	Ir-Pt(210)	Pt(310)	Ir-Pt(310)	Pt(410)	Ir-Pt(410)
$N_2 + * \rightarrow N_2*$	0.30	0.16	0.22	0.11	0.23	0.11
$N_2* + * + H^+ + e^- \rightarrow N_2H**$	1.19	1.16	1.16	1.15	1.16	1.14
$N_2H** + H^+ + e^- \rightarrow N_2H_2**$	0.27	0.02	0.18	-0.06	0.16	-0.07
$N_2H_2** \rightarrow 2NH*$	-0.33	-0.57	-0.73	-0.92	-0.72	-0.91
$NH* + H^+ + e^- \rightarrow NH_2*$	-0.36	-0.27	-0.21	-0.15	-0.21	-0.14
$NH_2* + H^+ + e^- \rightarrow NH_3*$	-0.60	-0.58	-0.65	-0.52	-0.64	-0.53
$NH_3* \rightarrow NH_3 + *$	0.04	0.26	0.24	0.33	0.23	0.32

a

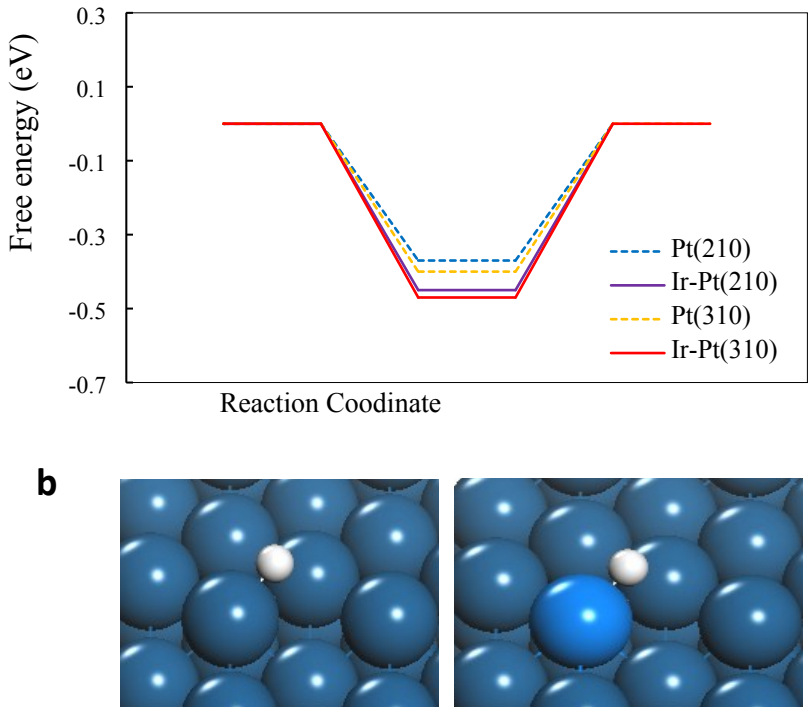

Fig. S14. (a) Free energy profiles for hydrogen evolution reactions (HER) on Pt and Ir modified Pt surfaces under the standard hydrogen electrodes condition. (b) Optimized structures of H* on Pt and Ir modified Pt surfaces

It was well known that the binding free energy of H* was widely applied as an activity descriptor for HER; the optimal catalysts should have a moderate value of ~0 eV. The free energy profiles in HER (Figure S14a) clearly displayed that the presence of Ir enhance the H* adsorption on (210) or (310) by ~0.08 eV, leading to even worse HER activities in comparison with pure Pt. This well agrees with the experimental findings that the hindered HER on PtIr. The calculated H* adsorption energies ($H^+ + e^- \rightarrow H^*$) are listed in Table S3.

Table S4. The binding free energy of H* on different

	Pt(210)	PtIr(210)	Pt(310)	PtIr(310)
H* adsorption energy	-0.37	-0.45	-0.40	-0.47

REFERENCES

(S1) L. Wei, Y.-J. Fan, H.-H. Wang, N. Tian, Z.-Y. Zhou and S.-G. Sun, *Electrochim. Acta,* 2012, **76**, 468.

(S2) L. Wei, B.-A. Lu, M.-J. Sun, N. Tian, Z.-Y. Zhou, B.-B. Xu, X.-S. Zhao, and S.-G. Sun, *Nano Res.,* 2016, **9**, 3547.

(S3) L. Wei, K. Liu, Y.-J. Mao, T. Sheng, Y.-S. Wei, J.-W. Li, X.-S. Zhao, F.-C. Zhu, B.-B. Xu, and S.-G. Sun, *Phys. Chem. Chem. Phys*., 2017, **19**, 31553.

(S4) D. Zhu, L. Zhang, R. E. Ruther, and R. J. Hamers, *Nat. Mater.,* 2013, **12**, 836.

(S5) G. W. Watt, and J. D. Chrisp, *Anal. Chem.,* 1952, **24**, 2006.

(S6) J. M. Soler, E. Artacho, J. D. Gale, A. Garcia, J. Junquera, P. Ordejon, D. Sanchez-Portal, *J. Phys.: Condens. Matter,* 2002, **14**, 2745.

(S7) J. Junquera, O. Paz, D. Sanchez-Portal, and E. Artacho, *Phys. Rev. B,* 2001, **64**, 235111.

(S8) N. Troullier, and J. L. Martins, *Phys. Rev. B,* 1991, **43**, 1993.

(S9) J. P. Perdew, K. Burke, and M. Ernzerhof, *Phys. Rev. Lett.,* 1996, **77***,* 3865.

(S10) M. Dion, H. Rydberg, E. Schroder, D. C. Langreth, and B. I. Lundqvist, *Phys. Rev. Lett.,* 2004, **92**, 246401.

(S11) G. Roman-Perez, and J. M. Soler, *Phys. Rev. Lett.,* 2009, **103**, 096102.

(S12) J. K. Norskov, J. Rossmeisl, A. Logadottir, L. Lindqvist, J. R. Kitchin, T. Bligaard, and H. Jonsson, *J. Phys. Chem. B,* 2004, **108***,* 1520.

(S13) A. A. Gokhale, S. Kandoi, J. P. Greeley, M. Mavrikakis, and J. A. Dumesic, *Chem. Eng. Sci.,* 2004, **59**, 4679.

(S14) D. Yang, T. Chen, and Z. Wang, *J. Mater. Chem. A,* 2017, **5**, 18967.

(S15) S. Chen, S. Perathoner, C. Ampelli, C. Mebrahtu, D. Su, and G. Centi, *Angew. Chem. Int. Ed.,* 2017, **56**, 2699.

(S16) D. Bao, Q. Zhang, F. L. Meng, H. X. Zhong, M. M. Shi, Y. Zhang, and X. B. Zhang, *Adv. Mater*. 2017, **29**, 1604799.

(S17) M. Nazemi, and M. El-Sayed, *J. Phys. Chem. Lett*., 2018, **9**, 5160.

(S18) Q. Liu, X. Zhang, B. Zhang, Y. Luo, G. Cui, F. Xie, and X. Sun, *Nanoscale,* 2018, **10**, 14386.

(S19) J. Wang, L. Yu, L. Hu, G. Chen, H. Xin, and X. Feng, *Nat. Commun*., 2018, **9**, 1795.

(S20) Y. Song, D. Johnson, R. Peng, D. K. Hensley, P. V. Bonnesen, L. Liang, J. Huang, F. Yang, F. Zhang, R. Qiao, A. P. Baddorf, T. J. Tschaplinski, N. L. Engle, M. C. Hatzell, Z. Wu, D. A. Cullen, H. M. Meyer III, B. G. Sumpter, and A. J. Rondinone, *Sci. Adv.*, 2018, **4**, e1700336.

(S21) S. Mukherjee, D. A. Cullen, S. Karakalos, K. Liu, H. Zhang, S. Zhao, and G. Wu, *Nano Energy*, 2018, **48**, 217.

(S22) L. Zhang, X. Ji, X. Ren, Y. Luo, X. Shi, A. M. Asiri, B. Zheng and X. Sun, *ACS Sustain. Chem. Eng.*, 2018, **6**, 9550.

(S23) L. Zhang, X. Ji, X. Ren, Y. Ma, X. Shi, Z. Tian, A. M. Asiri, L. Chen, B. Tang and X. Sun, *Adv. Mater.*, 2018, **30**, 1800191.

(S24) R. Zhang, Y. Zhang, X. Ren, G. Cui, A. M. Asiri, B. Zheng and X. Sun, *ACS Sustain. Chem. Eng.*, 2018, **6**, 9545.

(S25) G. F. Chen, X. Cao, S. Wu, X. Zeng, L. X. Ding, M. Zhu and H. Wang, *J. Am. Chem. Soc.*, 2017, **139**, 9771.

(S26) H. Huang, L. Xia, X. Shi, A. M. Asiri and X. Sun, *Chem. Commun.*, 2018, **54**, 11427.

(S27) L. Zhang, X. Ren, Y. Luo, X. Shi, A. M. Asiri, T. S. Li and X.-P. Sun, *Chem. Commun.*, 2018, **54**, 12966.

(S28) X. Yu, P. Han, Z. Wei, L. Huang, Z. Gu, S. Peng, J. Ma and G. Zheng, *Joule*, 2018, **2**, 1610.

(S29) L. Hu, A. Khaniya, J. Wang, G. Chen, W. E. Kaden and X. Feng, *ACS Catal.*, 2018, **8**, 9312.

(S30) J. Han, X. Ji, X. Ren, G. Cui, L. Li, F. Xie, H. Wang, B. Li and X. Sun, *J. Mater. Chem. A*, 2018, **6**, 12974.

(S31) X. Ren, G. Cui, L. Chen, F. Xie, Q. Wei, Z. Tian and X. Sun, *Chem. Commun.*, 2018, **54**, 8474.

(S32) X. Zhu, Z. Liu, Q. Liu, Y. Luo, X. Shi, A. M. Asiri, Y. Wu and X. Sun, *Chem. Commun.*, 2018, **54**, 11332.

(S33) X. Zhang, Q. Liu, X. Shi, A. M. Asiri, Y. Luo, X. Sun and T. Li, *J. Mater. Chem. A*, 2018, **6**, 17303.

(S34) J. Kong, A. Lim, C. Yoon, J. H. Jang, H. C. Ham, J. Han, S. Nam, D. Kim, Y.-E. Sung, J. Choi and H. S. Park, *ACS Sustain. Chem. Eng.*, 2017, **5**, 10986.

(S35) V. Y. Evtushok, A. N. Suboch, O. Y. Podyacheva, O. A. Stonkus, V. I. Zaikovskii, Y. A. Chesalov, L. S. Kibis and O. A. Kholdeeva, *ACS Catal.*, 2018, **8**, 1297.

(S36) C. Lv, C. Yan, G. Chen, Y. Ding, J. Sun, Y. Zhou and G. Yu, *Angew. Chem. Int. Ed.*, 2018, 57, 6073.

(S37) Y. Zhang, W. Qiu, Y. Ma, Y. Luo, Z. Tian, G. Cui, F. Xie, L. Chen, T. Li and X. Sun, *ACS Catal.*, 2018, **8**, 8540.

(S38) W. Qiu, X. Y. Xie, J. Qiu, W. H. Fang, R. Liang, X. Ren, X. Ji, G. Cui, A. M. Asiri, G. Cui, B. Tang and X. Sun, *Nat. Commun.*, 2018, **9**, 3485.

(S39) J. Han, Z. Liu, Y. Ma, G. Cui, F. Xie, F. Wang, Y. Wu, S. Gao, Y. Xu and X. Sun, *Nano Energy*, 2018, **52**, 264.

(S40) L. Zhang, L. X. Ding, G. F. Chen, X. Yang and H. Wang, *Angew. Chem. Int. Ed.*, 2019, **58**, 2612.

(S41) L. Han, X. Liu, J. Chen, R. Lin, H. Liu, F. Lu, S. Bak, Z. Liang, S. Zhao, E. Stavitski, J. Luo, R. R. Adzic and H. Xin, *Angew. Chem. Int. Ed.*, 2019, **58**, 2321.

(S42) Y. Wang, X. Cui, J. Zhao, G. Jia, L. Gu, Q. Zhang, L. Meng, Z. Shi, L. Zheng, C. Wang, Z. Zhang and W. Zheng, *ACS Catal.*, 2019, **9**, 336.

(S43) M.-M. Shi, D. Bao, S.-J. Li, B.-R. Wulan, J.-M. Yan and Q. Jiang, *Adv. Energy Mater.*, 2018, **8,** 1800124.

(S44) H. Tao, C. Choi, L.-X. Ding, Z. Jiang, Z. Han, M. Jia, Q. Fan, Y. Gao, H. Wang, A. W. Robertson, S. Hong, Y. Jung, S. Liu and Z. Sun, *Chem*, 2019, **5**, 204.

(S45) X. Yang, K. Li, D. Cheng, W.-L. Pang, J. Lv, X. Chen, H.-Y.Zang, X.-L. Wu, H.-Q. Tan, Y.-H. Wang and Y.-G. Li, *J. Mater. Chem. A*, 2018, **6**, 7762.

(S46) Z. Wang, Y. Li, H. Yu, Y. Xu, H. Xue, X. Li, H. Wang and L. Wang, *ChemSusChem*, 2018, **11**, 3480.

(S47) M. M. Shi, D. Bao, B. R. Wulan, Y. H. Li, Y. F. Zhang, J. M. Yan and Q. Jiang, *Adv. Mater.*, 2017, **29**, 1606550.

(S48) H.-M. Liu, S.-H.Han, Y. Zhao, Y.-Y.Zhu, X.-L.Tian, J.-H.Zeng, J.-X. Jiang, B. Y. Xia and Y. Chen, *J. Mater. Chem. A*, 2018, **6**, 3211.

(S49) C. Lv, Y. Qian, C. Yan, Y. Ding, Y. Liu, G. Chen and G. Yu, *Angew. Chem. Int. Ed.*, 2018, **57**, 10246.